Dynamics and storage of brine in mid-ocean ridge hydrothermal systems

Fabrice J. Fontaine[1] and William S. D. Wilcock[1]

Received 3 June 2005; revised 26 January 2006; accepted 20 February 2006; published 16 June 2006.

[1] Mid-ocean ridge hydrothermal systems are known to vent fluids with salinities substantially different from seawater as a result of phase separation and segregation of the resulting vapor and brine phases. Time series of vent temperature and salinity (chlorinity) show that some black-smoker vent fields such as the Main Endeavour Field on the Juan de Fuca Ridge have vented fluids with salinities well below seawater for over a decade, which raises important questions concerning the fate of brines in these systems. One widely accepted model is that high-density brines formed by supercritical phase separation sink to the base of hydrothermal systems, leading to the development of a two-layer system in which a recirculating brine layer underlies a single-pass seawater cell. We first present theoretical arguments to constrain the dynamics of such a deep brine layer in a system still undergoing phase separation, and we conclude that if brines are stored in a basal layer, they are unlikely to convect because they will be stably stratified. One consequence of this result is that the brine layer beneath black smoker systems has to be thin (<10 m) to match the high heat fluxes. However, estimates of the rate at which brines are accumulating in the crust below the main field on the Endeavour segment of the Juan de Fuca Ridge suggest that the brine layer is likely at least 100 m thick. To resolve this apparent paradox, we propose an alternative model. We argue that interfacial tensions between fluid and solid phases will likely favor the segregation of vapor into the main fractures and brine into the smaller fissures and backwaters. This allows the vapor to flow efficiently through the system and transport large heat fluxes while most of the porosity in the lower part of the system fills with brines. It is generally believed that the pressure gradients in mid-ocean ridge hydrothermal systems are close to cold hydrostatic. At the high temperatures and pressures characteristic of the deeper parts of these systems, brines with salinities as high as 20 wt % NaCl have densities around 800–900 kg m^{-3} and will be buoyant in a cold-hydrostatic system. Rather than sinking to the base of the system, it is possible that brines produced by supercritical phase separation rise slowly until they reach a level of neutral buoyancy as they cool or enter high-permeability regions in which the pressure gradients decrease.

Citation: Fontaine, F. J., and W. S. D. Wilcock (2006), Dynamics and storage of brine in mid-ocean ridge hydrothermal systems, *J. Geophys. Res.*, *111*, B06102, doi:10.1029/2005JB003866.

1. Introduction

[2] The salt (chloride) contents of hot fluids venting from mid-ocean ridge hydrothermal systems generally differ from seawater with reported salinities ranging from 10% to 200% seawater [*VonDamm*, 1995]. Some early studies focused on precipitation-dissolution processes that could influence the chloride content of hydrothermal fluids [*Edmond et al.*, 1979; *Seyfried et al.*, 1986], but it has been long accepted that these salinity variations in hydrothermal fluids are primarily due to phase separation [*Delaney et al.*, 1987; *Cowan and Cann*, 1988; *VonDamm*, 1988; *Bischoff and Rosenbauer*, 1989]. Both subcritical and supercritical phase separation are required to explain the variability in vent salinities [e.g., *VonDamm and Bischoff*, 1987; *VonDamm*, 1988; *Butterfield et al.*, 1990]. *VonDamm* [1988] argues that vent salinities can be explained by the mixing of seawater with either a gas-free brine or a gas-rich vapor formed by phase separation deeper in the system.

[3] Further evidence for phase separation comes from the analysis of fluid inclusions trapped in hydrothermal minerals. Although many high-salinity (~50 wt % NaCl) inclusions are thought to be of magmatic origin [*Kelley et al.*, 1992, 1993; *Kelley and Früh-Green*, 2001], low- to moderate-salinity inclusions (<1.0 and up to 15–20 wt % NaCl) have been attributed to phase separation followed by the segregation of the vapor and brine phases [*Nehlig*, 1991; *Kelley et al.*, 1992, 1993; *Saccocia and Gillis*, 1995]. Segregation results from the buoyancy contrast between

[1]School of Oceanography, University of Washington, Seattle, Washington, USA.

0148-0227/06/2005JB003866$09.00

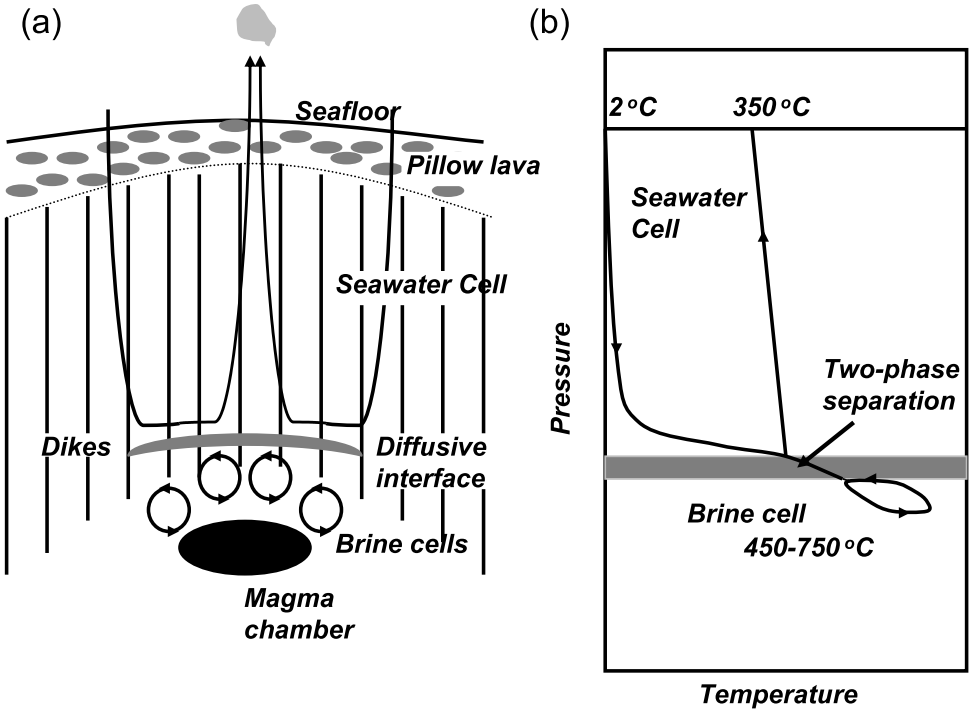

Figure 1. Schematic diagram showing the two-layer double-diffusive hydrothermal system envisioned for mid-ocean ridges by *Bischoff and Rosenbauer* [1989]. (a) Cross section showing the configuration of the two layers of circulation overlying the axial magma chamber. A recirculating brine layer formed by the supercritical phase separation of seawater underlies a single pass seawater cell. The two layers are separated by a thin interface through which heat and salt diffuse. (b) Temperature distribution envisioned for the model. In the seawater cell, cold seawater descends, heats up into the two-phase region, and ascends to feed black smoker vents. The brine layer circulates at temperatures of 450–750°C.

the two phases and from the nonuniform crustal porosity and permeability distributions [*Goldfarb and Delaney*, 1988; *Fox*, 1990]. Low-salinity, low-density vapors are expected to ascend buoyantly in the system, mix with cooler seawater, and then vent at the seafloor producing low-salinity (compared to seawater) vents.

[4] The fate of higher salinity brines is less obvious. The presence of high-salinity vents proves that fluids with salinities greater than seawater can be flushed at the seafloor. Whether these fluids are formed at the venting salinity [*VonDamm et al.*, 1997] or are the product of mixing between higher salinity brines and seawater [*VonDamm and Bischoff*, 1987; *VonDamm*, 1988; *Butterfield and Massoth*, 1994] remains unclear. The temporal progression of vent salinities following diking-eruptive events [*VonDamm et al.*, 1997; *Butterfield et al.*, 1997] commonly shows an evolution from vapor-dominated to brine-dominated venting, indicating that brines are stored in the crust at least temporarily. Some vents have been venting low-salinity fluids for many years and the venting of the brine has never been observed. For example, hydrothermal vents at the Main Endeavour Field of the Juan de Fuca Ridge have vented low-salinity fluids from 1984 to present [*Butterfield et al.*, 1994; *Lilley et al.*, 2003]. At the Bio9 site at 9°50′N on the East Pacific Rise hydrothermal vents have vented low-salinity fluids since 1991 [*VonDamm*, 2004].

[5] From a study of the chlorine (Cl/K ratio) content of mid-ocean ridge basalt glasses, *Michael and Cornell* [1998] come to the conclusion that the high Cl/K ratios found in samples from intermediate and fast spreading are due to the assimilation of Cl-rich crust during crystallization in a shallow magma chamber. They hypothesize that the Cl enrichment is a result of brines formed by phase separation of seawater, an idea that is supported by the seawater-like $^{37}Cl/^{35}Cl$ isotopic ratios of the glasses [*Magenheim et al.*, 1995]. Thus it appears that brines may accumulate in the deepest parts of the crust near the magma crystallization interface.

[6] *McNabb and Fenner* [1985] argue that dense brines formed by supercritical phase separation accumulate as a stratified layer at the base of the hydrothermal system beneath the convecting seawater layer. While the layer grows the venting fluids are vapor-dominated. If the brine layer becomes too thick and cools at its top, seawater circulation dissolves salt and reduces its thickness. The venting of brine-dominated or vapor-dominated fluids is thus separated in time but not necessarily in space. The brine layer is initially stably stratified but they argue that it could potentially convect. *Bischoff and Rosenbauer* [1989] build upon these ideas and propose that double-diffusion processes break the stratification of the brine layer and generate convective motions. In their model, mid-ocean ridges hydrothermal systems are composed of a single pass seawater cell overlying a dense, high-temperature brine cell with salinities that are at least five times seawater (Figure 1).

[7] *Lowell and Germanovich* [1997] use a conductive heat balance to estimate a thickness of 1–10 m for the brine layer. They argue that such layers can form in less than a year and suggest that the continuous venting of high-chlorinity fluids on timescales of decades could be the result of the depletion of the brine layer by diffusion into the overlying seawater layer. Recently, *Schoofs and Hansen* [2000] model the depletion of a basal brine layer in a convecting system that has cooled to the single-phase regime (<400°C). They find that the interface between the two layers is unstable and vanishes by one of two dynamical mechanisms: convective breakdown and vertical migration. If the brine layer envisioned by *McNabb and Fenner* [1985] or *Bischoff and Rosenbauer* [1989] was to cool down, it will be depleted at a much faster rate than predicted for pure diffusion.

[8] Since the model of *Schoofs and Hansen* [2000] is valid only when a two-layer system has cooled into the single-phase region, it does not address the mechanism by which such systems form nor is it appropriate for the high-temperature black smoker systems which clearly circulate into the two-phase region. One approach to understanding such systems is to develop numerical models of two-phase flow. Such models are challenging because they require significant computational resources and a self-consistent and accurate equation of state and are dependent upon assumptions about the dynamical behavior of two phase mixtures. To date, a few two-phase models of mid-ocean ridges hydrothermal systems have been developed. *Bai et al.* [2003] construct one-dimensional heat pipe solutions for H_2O-NaCl fluids and explore the effect of basal heat flux and permeability on their behavior. They derive the fluid properties using the relationships of *Palliser and McKibbin* [1998a, 1998b, 1998c] but avoid a region around the critical point where the relationships lead to inconsistent fluid properties. Their model is the first to show the production and accumulation of brine at the base of mid-ocean ridge hydrothermal systems. *Kawada et al.* [2004] develop two-dimensional models in which they use an equation of state derived from *Anderko and Pitzer* [1993]. Although their models do not include a complete description of two-phase flow, they infer that phase separation leads to the formation of a two-layer system. Seawater vigorously circulates in an upper layer while a stagnant brine-rich two-phase zone forms at the base of the system. They predict that fluids venting at the ridge axis will have salinities greater than those venting just off-axis. *Geiger et al.* [2004] also develop two-dimensional, two-phase flow models of magmatic hydrothermal systems in which they use their own equation of state [*Driesner and Heinrich*, 2003]. They identify five general flow patterns from single-phase diffusive to two-phase convective. They argue that brines in the two-phase flow regime remain immobile because of their high density and low volume fraction.

[9] In this study, we follow an alternative approach to investigate the dynamics and storage of supercritical brines in mid-ocean ridge hydrothermal systems. Although the two-layer model of *Bischoff and Rosenbauer* [1989] is widely accepted there is no conclusive evidence for such a configuration. In particular, the assumption that the brine layer can convect in the two-phase regime is not obviously correct and is inconsistent with at least one of the two-phase numerical models [*Kawada et al.*, 2004]. In this paper, we first discuss theoretical constraints on the dynamics of the brine layer envisioned by *Bischoff and Rosenbauer* [1989] and conclude that phase separation leads to a stably stratified rather than a convective brine layer. We then consider the field constraints and infer that the presence of such a layer at the base of smoker-like hydrothermal systems is difficult to reconcile with the large heat flux typical of these systems. We argue for an alternative model for subsurface brine storage at mid-ocean ridges in which the brines preferentially enter the smaller cracks and backwaters of the permeable system and in which brines with significant salinities may actually upwell instead of pooling at the base of the hydrothermal system.

2. Constraints on the Dynamics of Brine Layer

2.1. Physical Conditions in Mid-ocean Ridge Hydrothermal Systems

[10] The structure of the crust at mid-ocean ridges can be approximated by a layered system comprising extrusive pillow basalts, sheeted dikes and a plutonic-gabbroic unit overlying the mantle. At fast and medium spreading ridges, seismic reflection studies image a sill-like, axial magma lens below the dikes approximately 1–3 km below the seafloor (see *German and Lin* [2004] for a short review). These axial melt lenses typically extend ~1 km across axis [e.g., *Kent et al.*, 1990], are about 10- to 100-m-thick [e.g., *Singh et al.*, 1998] and have been followed along axis continuously for lengths tens of kilometers [e.g., *Detrick et al.*, 1987]. They are partially or fully molten with temperatures in excess of 1200°C and overly a thick zone of low seismic velocity interpreted as a crystal mush zone. The transition between the sheeted dike complex and the melt lens comprises a thin gabbroic section a few tens to hundreds meters thick [*Singh et al.*, 1999; *Toomey et al.*, 1994]. With the exception of the hot spot-influenced Reykjanes Ridge [*Sinha et al.*, 1997], slow spreading ridges usually lack an axial melt lens. However, a thick low-velocity zone interpreted as a crystal mush is present [e.g., *Magde et al.*, 2000].

[11] Hydrothermal fluids circulate in mid-ocean ridges crust through a network of fissures and fractures. At the ridge axis, this network results from the brittle fracturing of the rocks under the tensional stress resulting from seafloor spreading. The vertical depth of fracturing is controlled by the brittle-ductile transition which likely occurs at temperatures of about 700–750°C [*Hirth et al.*, 1998]. At the axis of fast and medium spreading rate ridges, these temperatures are encountered in the transition zone immediately above the axial melt lens at a depth of 1–3 km below the seafloor. At slow spreading axis, earthquake focal depths of several kilometers (up to 10 km on the Mid-Atlantic Ridge [*Toomey et al.*, 1985; *Wolfe et al.*, 1995]) indicate that the entire crust may be sufficiently cold to fracture.

[12] This temperature of 700–750°C at the brittle-ductile transition has long been equated to the maximum temperature reached by seawater-derived hydrothermal circulation [*Gillis et al.*, 2001]. However, recent studies have found evidence for very high temperature alteration (~1000°C) in gabbroic layers of the Oman ophiolites [*Manning et al.*, 2000; *Nicolas et al.*, 2003; *Bosch et al.*, 2004]. The alteration is found in a microcrack network which is assumed to be part of a recharge area that was located

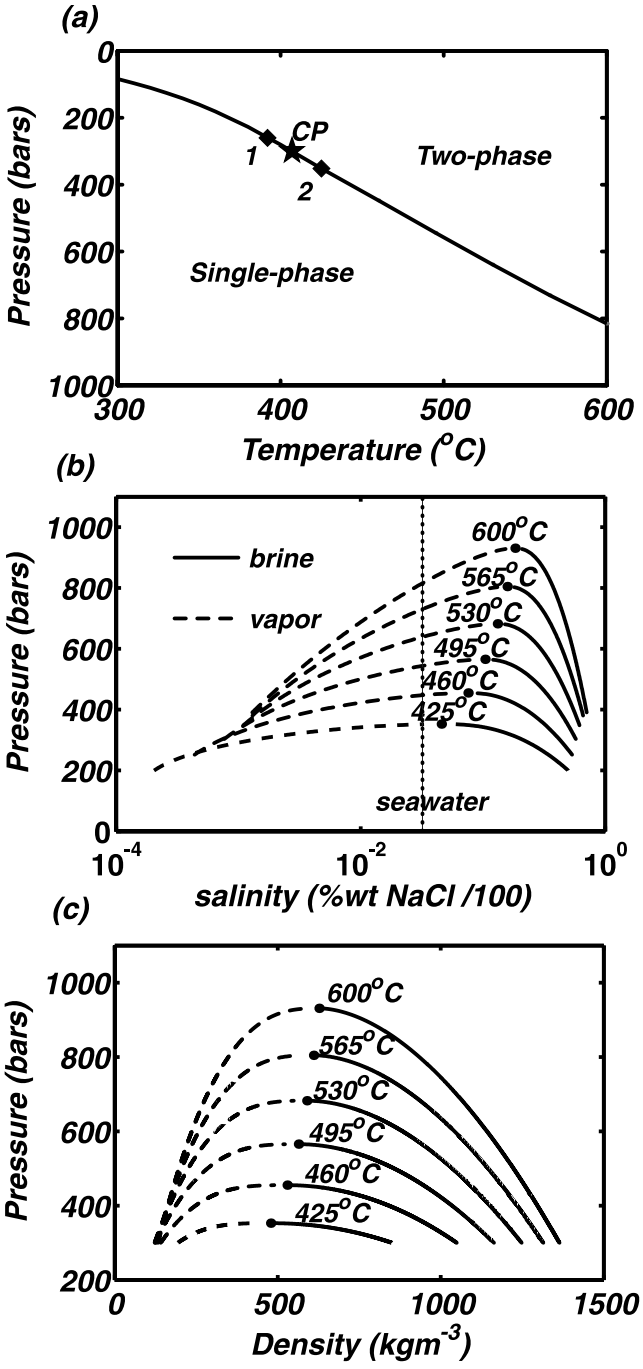

Figure 2. (a) Two-phase boundary for seawater (~3.2 wt % NaCl). The critical point (CP) is at 407°C and 300 bars. In the subcritical region (e.g., point 1), vapor droplets boil from seawater. In the supercritical region (e.g., point 2), brine droplets condense from seawater. (b) Salinity, temperature, and pressure relationships for the NaCl-H_2O system in the two-phase area. Phase salinities are shown for six temperatures ranging from 425 to 600°C. Vapor and brine salinities are plotted as dashed and solid lines, respectively. Seawater salinity is also shown as a dotted line at 3.2 wt % NaCl. (c) Same as Figure 2b but for density.

several kilometers off the axis of the fast spreading ridge [*Nicolas et al.*, 2003]. This recharge zone allowed seawater to circulate to the walls of the cooling magma chamber where hydrous melting was triggered. The discharge system consists of a network of clinopyroxene, pargasite gabbroic dikes formed by the hydrous melting [*Nicolas et al.*, 2003]. *Nicolas et al.* [2003] argue that the microcrack network formed in the ductile regime due to the anisotropy of thermal contraction as gabbros cooled from 1200 to 700°C. It is unclear whether very high temperature circulation occurs at the ridge axis. Field observations have constrained the highest temperature of axial hydrothermal alteration to ~700–750°C [*Gillis et al.*, 2001; *Vanko and Stakes*, 1991; *Manning et al.*, 1996], in agreement with the temperature at the brittle-ductile transition.

2.2. Two-Layer Model

[13] *Bischoff and Rosenbauer* [1989] argue that the base of mid-ocean ridge hydrothermal systems is occupied by brines. According to their model, the brine is generated by supercritical phase separation of seawater in the deeper parts of the system where temperatures and pressures are significantly higher than the critical point of seawater (407°C, 300 bars, Figure 2a). Supercritical phase separation leads to the condensation of small droplets of dense, saline brines that coexist with low-salinity, low-density vapors. As the vapors buoyantly segregate from the brine and are flushed at the seafloor, the brine layer builds up and stratifies. During this time the salinities of venting fluids are lower than seawater. The accumulation of brines at the base of the system ultimately stops the supercritical phase separation process by preventing seawater from reaching the deepest and hottest part of the system. Then the system reaches an equilibrium in which a "mature" two-phase brine layer underlies a single-phase seawater layer (Figure 1). The P-T conditions at the interface between the seawater and brine layers will then be a point on the Clapeyron curve for seawater (Figure 2a). *Bischoff and Rosenbauer* [1989] infer that the thicknesses of the brine layers are likely ~100–200 m. For bottom pressures ranging between 400 and 500 bars the equilibrium temperature at the interface between the brine and seawater layers is about 440–480°C (see Figure 2a) and the temperatures range between 450° and 700°C inside the newly formed supercritical layer.

[14] *Bischoff and Rosenbauer* [1989] argue that double-diffusion will break the stability of the layer and lead to a convecting brine layer. Double diffusive convection in porous media has been studied experimentally [*Griffiths*, 1981], theoretically [*Nield and Bejan*, 1992] and numerically [*Schoofs et al.*, 1998, 2000]. *Griffiths* [1981] shows analytically that necessary conditions for double-diffusive convection are that the fluid contains at least two components with different diffusivities (here, salt and temperature) and that these components make opposite contributions to the vertical density gradient. In an initially stable layer where both temperature and salinity increase with depth (Figure 3, profile i), salt will tend to diffuse upward, reducing the salinity and density at the base of the layer (Figure 3, profile ii) and thus enhancing convective instabilities. By this mechanism, the initial layer will break into a set of layers in which the salinity and temperature are constant and which are separated from each other by sharp

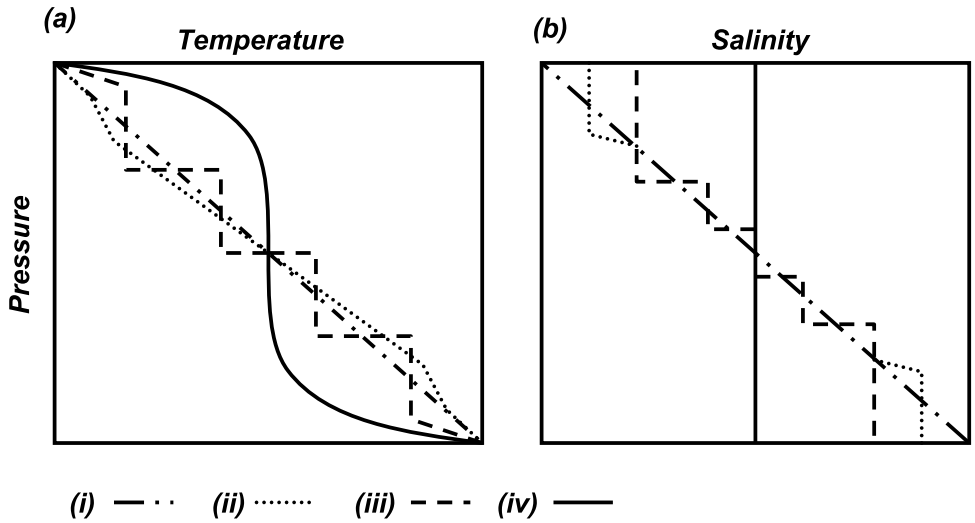

Figure 3. (a) Typical temperature versus pressure profiles during double-diffusive breakdown. (b) Same as Figure 3a but for salinity. Initially (profile i), the temperature and salinity distributions increase linearly with pressure. When convective instabilities are initiated at the base, the salinity and temperature distributions break into a series of layers separated by sharp diffusive interfaces (profiles ii and iii). Eventually, convective processes mix the whole layer (profile iv).

diffusive interfaces (Figure 3, profile iii). If the convection is sufficiently vigorous, these interfaces may ultimately disappear leading to a single, well-mixed convective layer; the salinity in the final layer being constant and equal to the mean salinity of the initial layer (Figure 3, profile iv). This is the configuration envisioned by *Bischoff and Rosenbauer* [1989]. Because of the salinity contrast, a thin diffusive interface separates the brine from the seawater layer. Brine heats the seawater through this interface and salt diffusion increases the salinity of the overlying upwelling hydrothermal fluids leading to venting salinities that are greater than seawater during intervals when there is no phase separation in the seawater layer.

2.3. Dynamics of Brine Layer: Convection Versus Conduction

[15] In order to investigate whether the supercritical brine layer is likely to convect when the system is in the two-phase regime, we conducted a stability analysis of the layer at temperatures ranging from 450 to 600°C and a bottom pressure of 500 bars. We assume that the brine layer has reached the mature state depicted by *McNabb and Fenner* [1985] and *Bischoff and Rosenbauer* [1989] (Figure 1) and sits on the two-phase curve everywhere while the vapor rises buoyantly out of the system. Such a configuration is likely to be appropriate for many black smokers that clearly circulate in the two-phase area. We used the equation of state of *Palliser and McKibbin* [1998b] to derive the density distribution inside the layer. During supercritical phase separation, the salinity of the brine and vapor phases is a function of temperature and pressure only (Figure 2b). The density of the brine phase is substantially higher than the density of the corresponding vapor (Figure 2c). At constant temperature, an increase in pressure leads to a decrease in the brine salinity and thus to a decrease in density. At constant pressure, an increase of temperature leads to an increase of the brine salinity and thus to an increase of its density. If one assumes a linear conductive temperature profile in the brine layer, the increase of pressure with depth will tend to destabilize the layer but the increase of temperature will tend to stabilize it. For a given layer thickness h or pressure change ΔP, it is possible to define a critical temperature variation ΔT below which the brine phase is unstable because the salinity (Figure 4a) and density (Figure 4b) decrease with depth. Figure 4c shows this critical temperature variation for layer thicknesses up to 2000 m and a bottom pressure of 500 bars. Similar results are found for bottom pressures of 400 bars. Layers that are a few hundreds meter thick are stable provided ΔT is greater than a few degrees Celsius, while layer with $\Delta T \sim 100$°C are unstable if h is about 2000 m. Clearly the brine layer envisioned by *Bischoff and Rosenbauer* [1989] will initially be stably stratified in the conductive regime because the small pressure variations (~10 bars) cannot overcome the stabilizing effect of large temperature variations (>50°C).

[16] *Bischoff and Rosenbauer* [1989] hypothesize that double-diffusive instabilities can break the stability of the layer but it is not clear whether this mechanism will work while the system sits on the two-phase curve. Consider a system that is analogous to profile i in Figure 3. If double-diffusion drives a salinity reduction at the base of the layer as shown on profile ii of Figure 3, the system will phase separate. The mean salinity will be lower because of the formation of the small amount of vapor but the salinity and density of the brine will remain unchanged. The buoyant vapor is likely to move upward, reequilibrating with the brines at shallow depths and lower temperatures before eventually escaping the brine layer. Thus double-diffusive salinity perturbations at the base of the system may generate a transient flow of vapor out of the layer but the brine will return to its stable configuration. This stabilizing mechanism has been observed in heat pipe models [*Bai et al.*, 2003].

[17] We also considered the expected brine density distribution along an idealized convective path (Figure 5). A

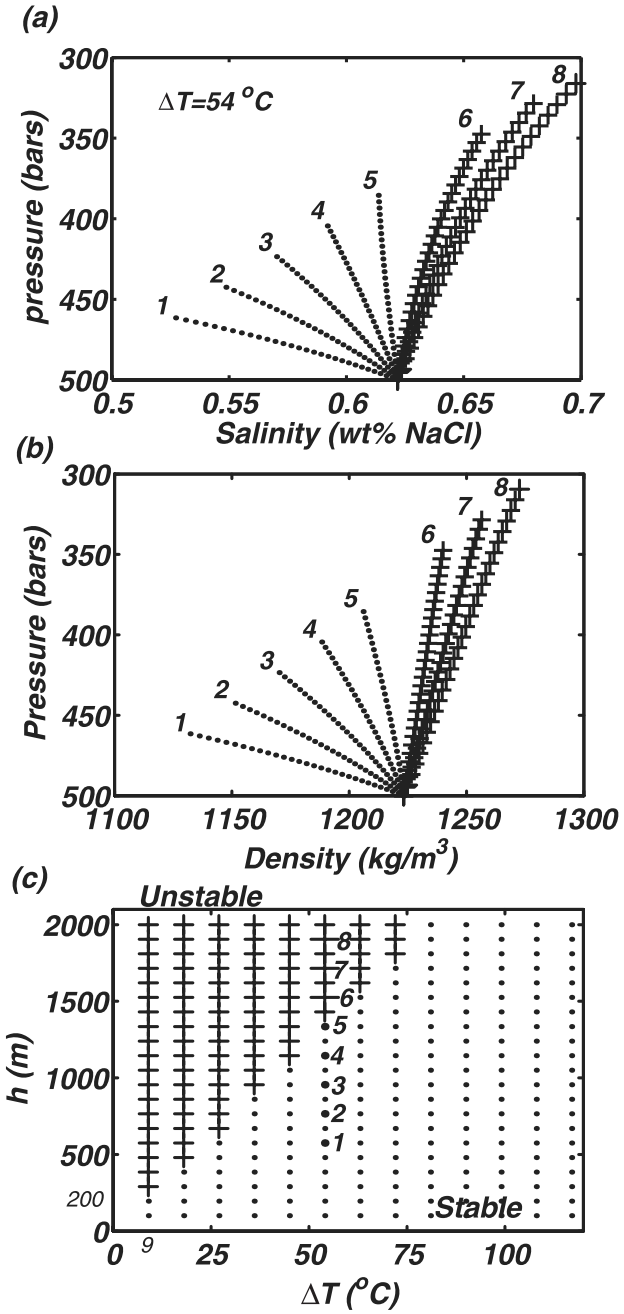

Figure 4. (a) Brine salinity as a function of pressure in a conductive layer. The temperature contrast ΔT across the layer is 54°C. The basal temperature and pressure are 600°C and 500 bars, respectively. The top temperature is 546°C. The eight curves represent eight different top pressures between 310 and 460 bars (1 = 460 bars; 2 = 440 bars; 3 = 425 bars; 4 = 405 bars; 5 = 385 bars; 6 = 350 bars; 7 = 330 bars; 8 = 310 bars). Depending on the top pressure, the brine salinity either increases (profiles 1–5) or decreases (profiles 6–8) with depth (pressure). (b) Same as Figure 4a but for brine density. (c) Stability of brine in the two-phase area for various layer thicknesses (h) and temperature contrasts (ΔT). Points and crosses represent stable and unstable configurations, respectively. Numbers refer to the eight profiles shown in Figures 4a and 4b. Inspection of the left-hand column of the stability determination (Figure 4c) shows that a 200-m-thick brine layer is stable for ΔT = 9°C or above.

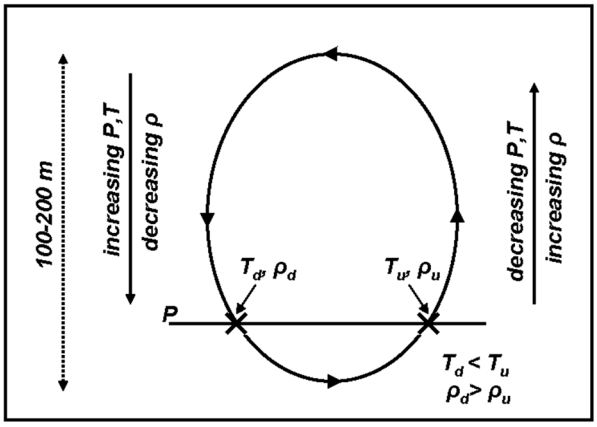

Figure 5. Typical temperature-pressure-density relationships along a convective path. In the downwelling part of the convective cell the fluid is heated up, temperature and pressure increase along the flow path, and density decreases. In the bottom boundary layer the temperature increases at almost constant pressure (horizontal flow) and density still decreases. In the upwelling region, the fluid cools down and the density decreases. Finally, in the top boundary layer the fluid moves horizontally, the temperature keeps decreasing, and the density increases. At a given pressure, the density in the upwelling zone ρ_u is always lower than the density in the downwelling zone ρ_d. Similarly, the temperature T_u in the upwelling zone is always greater than the temperature T_d in the downwelling zone.

convective cycle can be divided into four parts: a downwelling zone where the fluid slowly heats up, an upwelling zone where the fluid slowly cools down and two boundary layers where most of the heating and the cooling occurs. For a plausible convective path the fluid density should decrease as the fluid traverses the downwelling zone and bottom boundary layer and increase while it moves through the upwelling and top boundary layer. At any given depth the fluid density should be higher in the downwelling region than in the upwelling region (Figure 5). Because the salinity of the brine phase also increases with temperature at constant pressure (Figure 2b), brine density also increases (Figure 2c). Thus the brines in upwelling region of a convective cell will be denser than brines in downwelling region which is inconsistent with the density distribution required for convection.

[18] From the above considerations we infer that if the brines produced by supercritical phase separation are accumulating in a deep layer, this layer is unlikely to convect as long as the system remains hot enough to circulate in the two phase region. Observations from ophiolites often show relatively little hydrothermal alteration of the gabbro and dike sections where high-salinity fluids inclusions are found, which seems consistent with our inference [*Nehlig*, 1991; *Kelley et al.*, 1992].

3. Field Constraints on Brine Layer Thickness

[19] The Endeavour segment of the Juan de Fuca Ridge hosts five distinct high-temperature venting sites spaced

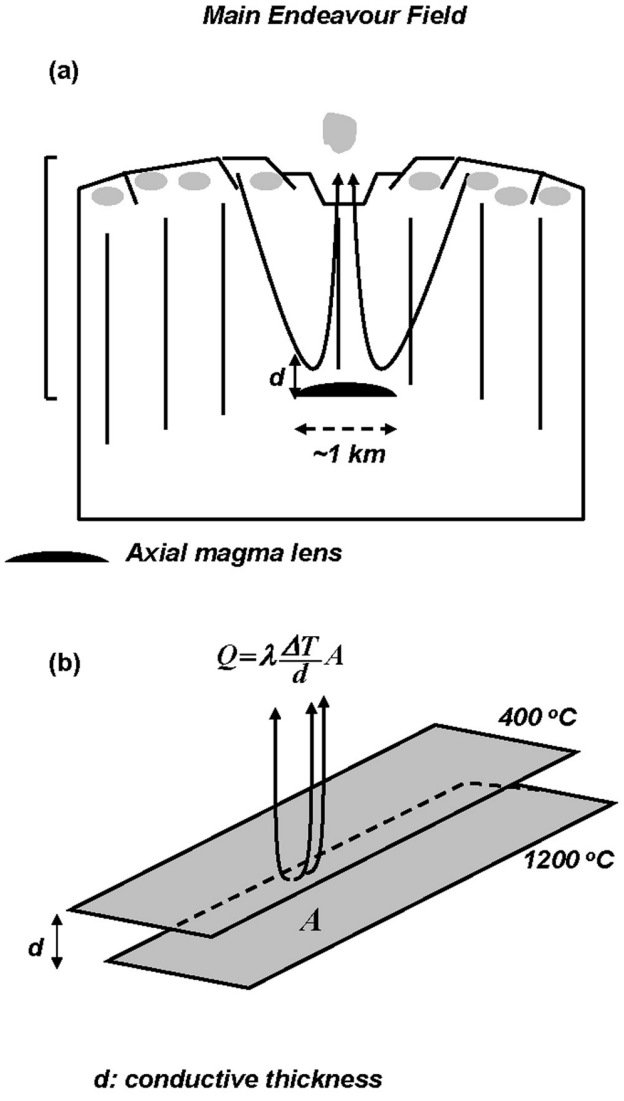

Figure 6. (a) Schematic diagram showing the geometry of hydrothermal circulation in the crust below the Main Endeavour Field. The depth to the axial magma lens is ~2.6 km [*Detrick et al.*, 2002; *Van Ark et al.*, 2003]. (b) Heat transfer across a conductive layer. The heat Q transferred through the layer depends on its thickness d according to Fick's law.

about 2–3 km apart along the central part of the segment. The water depth in the vent fields is about 2200 m and seismic refection profiles image the top of a magmatic lens 2.6 km below the seafloor [*Detrick et al.*, 2002; *Van Ark et al.*, 2003] (Figure 6a). The Main Endeavour Field was the first field to be discovered twenty years ago and has been studied extensively [*Delaney et al.*, 1992; *Butterfield et al.*, 1994]. The site hosts about a dozen structures and over 100 vents. The heat flux from the main field is 600 ± 50 MW and the ratio of the heat fluxes from focused and diffuse sources is estimated to be 6:1 [*Veirs et al.*, 2001].

[20] Temperature and chemistry time series show that each of the vent structures has a distinctive chemistry which remained almost constant between 1984 and 1999 [*Butterfield et al.*, 1994; *Lilley et al.*, 2003] until the system was perturbed by a volcanic event [*Johnson et al.*, 2000; *Lilley et al.*, 2003; *Seyfried et al.*, 2003]. For this period, maximum temperatures ranged from 360 to 380°C and the salinities varied across the field from 0.6 to 3 wt % NaCl. Following the 1999 event, the salinities of the freshest fluids increased substantially but all the vents continue to vent fluids with salinities below seawater. *Butterfield et al.* [1994] argue that the gradients in composition across the main field are consistent with supercritical phase separation. If the brine phase is accumulating at the base of the system and the venting fluids represent the vapors that segregate from these brines, a simple mass balance can be used to estimate the rate at which the brine layer is growing. One can write the total hydrothermal heat flux Q as

$$Q = Q_m C_p T \tag{1}$$

where Q_m is the associated total mass flux, C_p is the fluid heat capacity and T is the mean temperature of the flow. The mass flux of salt is simply $Q_m S_v$, where S_v is the mean fluid salinity (1.8 wt % NaCl). The salt mass flux lost due to brine storage is thus $Q_m(S - S_v)$, where S is the salinity of the initial single-phase fluid (seawater, 3.2 wt % NaCl). The volumetric rate V_t at which brine accumulates beneath the surface is

$$V_t = \frac{Q_m(S - S_v)}{S_b \rho_b} \tag{2}$$

where S_b is the brine salinity and ρ_b its density. After a time t, the thickness d of a vertical column of cross-sectional area A and porosity Φ is

$$d = V_t \frac{t}{\Phi A} = \frac{Q(S - S_v)}{C_p T S_b \rho_b} \frac{t}{\Phi A} \tag{3}$$

[21] For the main field the heat uptake area likely extends about 2 km along axis and 1 km across axis [e.g., *Wilcock and Fisher*, 2004]. If the brine accumulates in this region, the area A is 2 km^2. At a pressure of ~500 bars and for temperatures ranging between 500° and 600°C, brine salinities will be 25–65 wt % NaCl (Figure 2b). From equations (1) and (2) and with C_p = 5000 J kg^{-1} °C^{-1}, ρ_b = 1000 kg m^{-3} and the values of other parameters as outlined above we estimate that brines with such salinities would accumulate at a rate ranging from 0.007 to 0.018 m^3 s^{-1}. Assuming that the porosity in the lower dikes/uppermost gabbros is 2% [*Becker*, 1985], equation (3) predicts the brine layer at the base of the main field should grow at 5–13 m yr^{-1} or by 75–195 m between 1984 and 1999.

[22] The heat flux estimate of 600 ± 50 MW for the main field [*Veirs et al.*, 2001] can also be used to derive the thickness of a conductive brine layer. If the brine layer is stagnant the heat must be transferred through a conductive boundary layer extending from the roof of the axial magma chamber at ~1200°C across the brittle-ductile transition to the top of the brine layer at ~400–500°C (Figure 6b). The

thickness of the conductive boundary layer can be estimated using Fick's law according to

$$Q = \lambda \frac{\Delta T}{d} A \quad (4)$$

where ΔT is the temperature drop across the layer and λ is the rock thermal conductivity. Taking $\Delta T = 750°C$ and $\lambda = 2.5$ W m^{-1} °K^{-1} and the values of Q and A as outlined above, we estimate d $\sim$ 6 m. If the brittle-ductile transition is at 700°C, the thickness of the brine layer is $\sim$2 m.

[23] Clearly these two independent estimates of the expected thickness of a brine layer below the main field contradict one another: after 15 years of accumulation, the brine layer should be $\sim$100–200 m thick. However, if the brine layer is conductive as we infer, its thickness must be nearly 2 orders of magnitude lower to match the observed heat flux. These results lead us to question the two-layer model for the Endeavour system. One explanation is that brines are transported along axis where they mix with fluids in a "seawater" cell and vent at a different site. On the Endeavour segment the Mothra field to the south and the Salty Dawg and Sasquatch fields to the north fluids vent with salinities above seawater [David Butterfield, personal communication]. At the East Pacific Rise near 9°50′N, low-salinity fluids have also been observed for over a decade at vents such as Bio9 [*VonDamm*, 2004]. There are no heat flux estimates for this region that would allow us to duplicate the calculations presented for the Endeavour above but here a substantial amount of brine must also have been produced in the subsurface. *VonDamm* [2004] suggests that the brines flow downhill to the south before venting 10 km in a region where higher-salinity vents have been found.

[24] Another explanation is that brines flow across axis. Seismic data from the East Pacific Rise [*Dunn et al.*, 2000; *Crawford and Webb*, 2002] suggest that most of the plutonic section cools within a few kilometers of the ridge axis. Models of crustal accretion that include hydrothermal circulation and cooling [*Cherkaoui et al.*, 2003; *Chen*, 2004] show that this thermal structure requires that hydrothermal fluids circulate deep into the lower crust a few kilometers off axis. Thus dense brines could be removed from the ridge axis by flowing downslope into the lower crust. However, if the cracks are primarily oriented along axis such flow may be geometrically difficult.

[25] Although these explanations cannot be discounted, there is no conclusive evidence for such along or across axis brine transport. Moreover, the observation that vent fluids transition from vapor-dominated to brine-dominated on timescale of months to years after some magmatic events [*VonDamm et al.*, 1997; *Butterfield et al.*, 1997] indicates that brines are at least temporarily stored in situ at the ridge axis before being remobilized to vent in the region where they are formed. It is thus important to explore models to explain how such brines are stored.

4. A New Model for the Formation and Storage of Brine in the Crust

4.1. Relative Permeabilities and Interfacial Tensions

[26] It is generally accepted that the simultaneous porous flows of a liquid and its vapor in the two phase area can be described with an extension of Darcy's law [e.g., *Faust and Mercer*, 1979; *Ingebritsen and Hayba*, 1994; *Hayba and Ingebritsen*, 1997; *Xu and Lowell*, 1998; *Lewis and Lowell*, 2004]

$$q_i = -\frac{k_i}{\mu_i}(\nabla P - \rho_i g) \quad (5)$$

where subscript i refers to phase (v or b for vapor and brine, respectively), $\mathbf{q_i}$ is the Darcy velocity, k_i is the effective permeability, $\mathbf{g}$ is the gravity vector, P is the total pressure, ρ_i is the density and μ_i is the viscosity. The effective permeability is generally less than the intrinsic permeability and is different for the two phases. When both the brine and vapor phase are simultaneously present in the fractured basaltic matrix, the flow of each of them will be impeded by the presence of the other. This leads to a permeability reduction that is expressed in terms of relative permeability factors k_{ri} ($0 \leq k_{ri} \leq 1$), so that for a medium with an intrinsic permeability k, the effective permeability for phase i is $k_i = kk_{ri}$.

[27] The term k_{ri} is determined by the manner in which the two phases distribute themselves in the pores and this is controlled by interfacial tensions. In a porous medium, the molecules at the interface between a fluid and a solid or two fluids are submitted to cohesive forces from London-Van der Walls interactions and hydrogen bonds that reduce the tension of the interface and to adsorption forces operating across the interface itself that tend to increase the tension. The interfacial tension is determined by the balance of these forces. When two fluids are present, the intermolecular interactions between the two fluids and the solid results in a boundary angle (the wetting or contact angle, α) between the solid phase and the interface between the two fluids. The fluid with an acute boundary angle ($\alpha <$ 90°C) is said to "wet" the solid and is termed the wetting phase, while the other one is termed the nonwetting phase. When $\alpha = 0$, the wetting fluid will completely cover the solid surface.

[28] During the two-phase flow of pure water and steam it is known that liquid water wets the wall [*Helmig*, 1997; *Stumm*, 1992]. The polar water molecules in both phases are attracted toward the solid surface by the formation of hydrogen bonds, but because the liquid phase is denser it forms a higher density of hydrogen bonds and thus has a greater affinity to the rock walls. In brine-vapor flows it is generally assumed that brines wet the walls [*Scholl et al.*, 1993; *Lewis and Lowell*, 2004; *Geiger et al.*, 2004] although there are no experiments at high temperatures and pressures to confirm this. One reason for this is that the brines are denser. Furthermore, one can argue that when salt is dissolved in water, the ions (Na^+) will tend to be attracted toward the solid-liquid interfacial area by electrostatic interactions with the negatively charged rock walls. This will lead to a net flow of ions and the water molecules that are attracted to them by hydrogen bonds toward the solid-liquid interface, which will enhance the adhesion between the solid and the salty liquid. The formation of ion clusters at high temperature and pressure [*Oelkers and Helgeson*, 1991, 1993] may lower this effect by reducing the number of free Na^+ ions in the solutions. However, because the degree of ion association decreases with increasing density

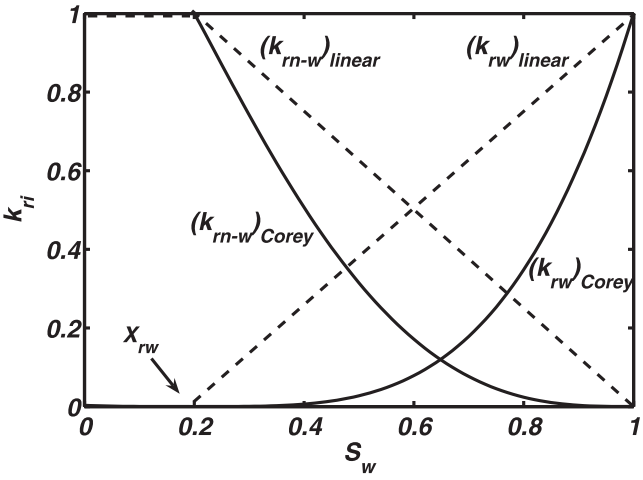

Figure 7. Relative permeability functions as a function of wetting phase saturation. Two sets of relative permeability functions are shown: linear (dashed lines) and Corey (thick lines) relationships. X_{rw} is the wetting phase residual saturation and corresponds to the minimum wetting phase saturation S_w for which k_{rw} is >0.

[*Oelkers and Helgeson*, 1991, 1993; *Driesner et al.*, 1991], it is likely that the proportion of ion pairs relative to free ions is greater in the vapor than in the brine. This effect may also enhance the electrostatic adhesion of brines to rock walls. In natural fractured media where the fissure apertures distribution is heterogeneous, the wetting phase will preferentially fill the smaller fissures, dead-ends and/or backwater porosity where its mobility is limited while the nonwetting phase will occupy the centers of the largest fissures.

[29] The relative permeabilities k_{ri} depend on the relative volumes of the two phases which can be expressed in terms of phase saturations X (that is the volume of one phase divided by the porous volume) which satisfy

$$X_w + X_{nw} = 1 \tag{6}$$

with subscripts w and nw now referring to the wetting and nonwetting phase, respectively. Theoretical [*Burdine*, 1953; *Mualem*, 1976] and experimental [*Brooks and Corey*, 1964; *Van Genutchen*, 1980] studies of various rock and soil types show that there is a critical wetting phase saturation below which only the nonwetting phase flows (Figure 7). The relative permeabilities may follow a linear relationship [*Romm*, 1966; *Horne et al.*, 2000] or a "Corey-type" relationship [*Wang and Horne*, 2000] (Figure 7). The sum of the two effective permeabilities is generally less than the intrinsic permeability indicating that the two phases impede each other.

[30] On the basis of these considerations, we infer that in the fractured basaltic rocks typical of mid-ocean ridges, brines preferentially occupy small fissures, dead-ends and backwater porosity as shown on Figure 8 (left). Should the brines saturation increase, brine may reach the larger fissures and line their walls confining the vapor to the fissure centers (Figure 8, bottom).

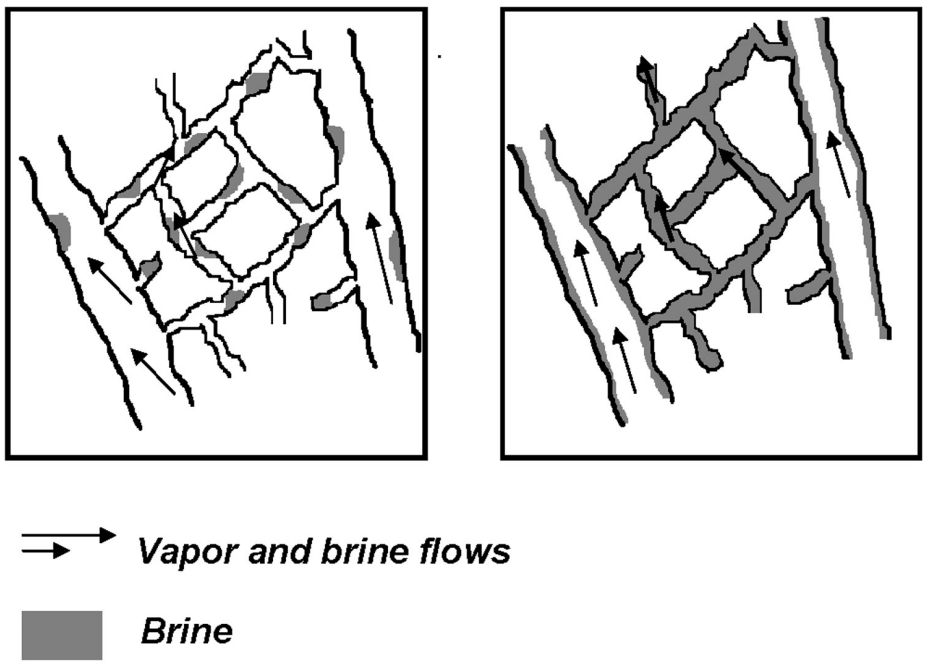

Figure 8. Expected wetting and nonwetting behaviors of brine and vapor in a fissured media. (left) At low brine saturations, brine preferentially fills dead-ends, backwater porosity, and small fissures, while vapors occupy the main fissures. (right) As brine saturation increases, it fills the backwater porosity and starts to coat the walls of the main fissures while vapor flows in the center.

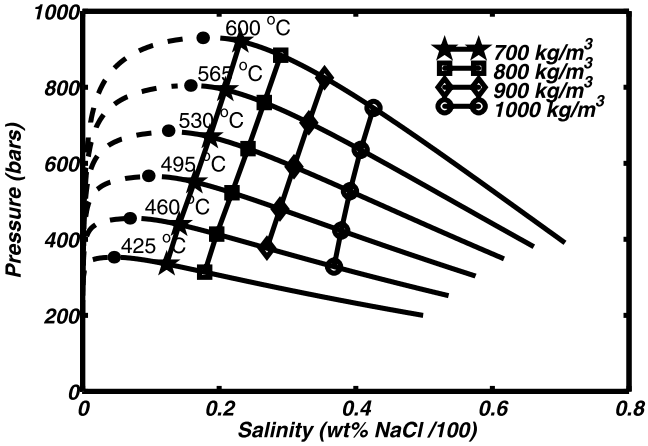

Figure 9. Temperature-pressure-salinity relationships in the two-phase area. Also plotted are the 700, 800, 900, and 1000 kg m^{-3} isopleths in the two-phase area. At temperatures greater than 400°C, brines with density lower than 800–900 kg m^{-3} have salinities between 20 and 30 wt % NaCl.

4.2. Brine Transport Directions

[31] The next issue is to understand the directions of the brine flow. Darcy's law (equation (5)) states that the horizontal flow of brine is governed by the pressure gradients with fluids moving from the high-pressure areas toward the low-pressure ones. The direction of the vertical flows is governed by the balance between the total vertical pressure gradient and the product $\rho_b g$ and satisfies

$$\text{Upward brine movement} \qquad \frac{1}{g}\frac{\partial p}{\partial z} > \rho_b, \tag{7}$$

$$\text{Downward brine movement} \qquad \frac{1}{g}\frac{\partial p}{\partial z} < \rho_b,$$

where the term $(1/g)(\partial p/\partial z)$ represents the local neutral density.

[32] Single pass hydrothermal systems can be schematically represented as two columns of different diameters representing the cold recharge and hot discharge areas [*Lowell and Germanovich*, 2004]. The vertical pressure gradient in the recharge and discharge zones is the sum of the local hydrostatic pressure gradients and the dynamic pressure gradient driving vertical flow. In a single pass system, the flow is near vertical everywhere except near the base of the system. If the permeability structure is continuous the horizontal pressure gradients between upflow and downflow zones must be small since otherwise such pres-

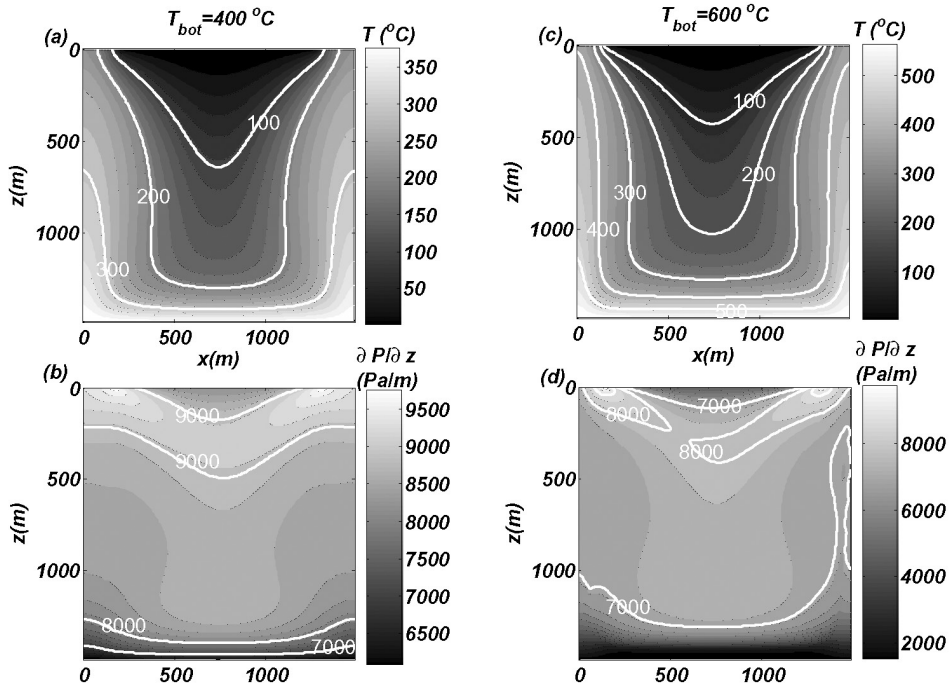

Figure 10. Two-dimensional temperature structure and pressure gradients obtained from two numerical experiments. (a) Temperature and (b) vertical pressure gradients for a model with a basal temperature equal to 400°C, $Nu = 3.3$ and $Ra = 600$. Exit temperatures are about 240°C. Pressure gradients at the base of upwelling zones (sides of the box) are >8000 Pa m^{-1} and increase upward. (c) and (d) Same as for Figures 10a and 10b except for a model with a basal temperature equal to 600°C, $Nu = 3.5$ and $Ra = 300$. Exit temperatures are about 370°C. Pressures gradients in upwelling zones are smaller than in the 400°C case (Figure 10c) and are lower than 7000 kg m^{-3} in most regions.

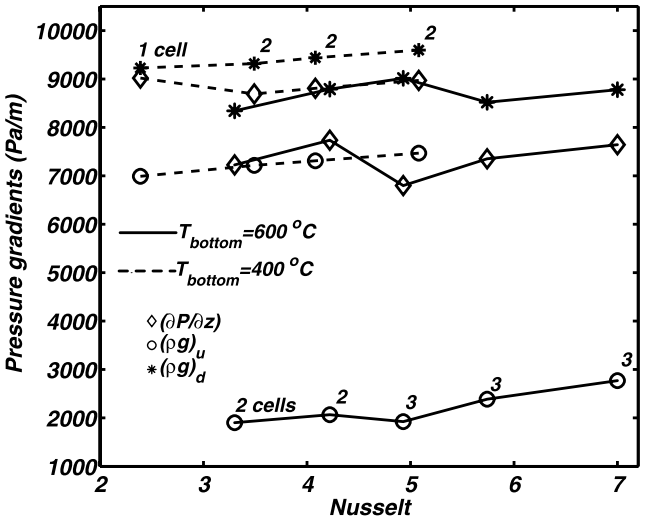

Figure 11. Pressure gradients as a function of Nusselt number. The term $(\rho g)_d$ is the maximum cold vertical hydrostatic pressure gradients at a depth of 1125 m (three fourths of the height of the model) in the dowwelling area; $(\rho g)_u$ is the same as $(\rho g)_d$ but for the hot vertical hydrostatic pressure gradients in the upwelling area; $\partial P/\partial z$ is the maximum computed vertical pressure gradient calculated at a depth of 1125 in the upwelling zone. The dashed and solid lines refer to experiments with basal temperature of 400°C and 600°C, respectively. For each solution, the number of cells is also listed. For a given number of cells, the pressure gradients tend to increase with *Nu.* The mean pressure gradient in the system is much closer to cold hydrostatic than hot hydrostatic.

sure gradients would drive horizontal flow. A balance of the volumetric fluid fluxes requires

$$\left(\frac{\partial P}{\partial z} - \rho_u g\right)\frac{k_u A_u}{\mu_u} = \left(\frac{\partial P}{\partial z} - \rho_d g\right)\frac{k_d A_d}{\mu_d} \tag{8}$$

where A represents cross-sectional areas and subscripts u and d refer to properties of the upflow and downflow zone, respectively. The terms in parentheses represent the dynamic pressure gradients driving upflow and downflow.

[33] A number of studies have considered the likely pressure gradients in mid-ocean ridge hydrothermal systems [*Cann and Strens*, 1989; *Wilcock and McNabb*, 1995; *Wilcock*, 1997; *Jupp and Schultz*, 2004; *Lowell and Yao*, 2002] and have reached the conclusion that they are probably close to cold hydrostatic. The results of limited numerical modeling [*Wilcock*, 1997] also suggest that the pressure gradients increase toward cold hydrostatic values with increasing Rayleigh number. The basal thermal boundary layer thins with increasing Rayleigh number which leads to a commensurate decrease in the width of upflow relative to downflow and hence to an increase in pressure gradients. Field observations show that the areas of vent fields [*Wilcock and McNabb*, 1995] and underlying high-temperature vertical upflow zones [*Cann and Strens*, 1989] are relatively small suggesting that even after allowing for the lower viscosity of upwelling fluids much larger pressure gradients are required to drive upflow than downflow. *Lowell and Yao* [2002] argue that anhydrite precipitation will clog the recharge zone unless recharge is distributed over a very large area.

[34] One important consequence of a system in which pressure gradients are close to cold hydrostatic or even midway between cold and hot hydrostatic is that hot, high-salinity brines may move upward rather than downward. Downwelling fluids at temperature $\leq$100°C will have densities of $\sim$950 kg m^{-3} while upwelling fluids at 350–400°C will have densities of $\sim$650 kg m^{-3}. If the ambient pressure gradient lies midway between cold and hot hydrostatic, fluids with densities $\leq$800 kg m^{-3} will upwell. If the system is circulating in the two-phase region this neutral density is equivalent to 10–20 wt % NaCl salinity (Figure 9). If the pressure gradients are close to cold hydrostatic, two-phase brines with salinities up to 30 wt % NaCl may be buoyant (Figure 9).

4.3. Numerical Investigations of Pressure Gradients

[35] In order to explore this idea further we ran a series of two-dimensional numerical models of hydrothermal circulation that build upon the work of *Wilcock* [1997] and *Jupp and Schultz* [2004]. The models are single phase and do not include the phase separation of seawater and the segregation of the vapor and brine phases. In the two-phase area we followed the approach adopted by *Wilcock* [1998] and assumed weighted mean properties of the brine and vapor phases. This approach is presumably accurate at least when only a small amount of brine is present in the system.

[36] The relevant conservation equations and solution techniques used are described in detail elsewhere [*Rabinowicz et al.*, 1998; *Fontaine et al.*, 2001]. We assume that the fluid flow obeys Darcy's law (equation (5)) and that the fluid and rock are always in thermodynamic equilibrium. The computational domain consists of a square box measuring 1.5 km $\times$ 1.5 km with an open top and a uniform 128 $\times$ 128 or 256 $\times$ 256 grid. The pressure at the top of the box is 300 bars. Fluid flow enters at 2°C and vents with a zero vertical temperature gradient. The base of the models is impermeable and the temperature is set to vary between 400° and 600°C. The temperature and pressure-dependent fluid density is obtained using the equation of state of *Pitzer et al.* [1984] at temperatures <300°C and *Anderko and Pitzer* [1993] at temperature >300°C. The viscosity of the hydrothermal fluid is derived using the relationship of *Meyer et al.* [1993].

[37] The governing equations are nondimensionalized and solved using an implicit finite difference method for the heat transport and a spectral decomposition technique for the flow [*Rabinowicz et al.*, 1998]. In the nondimensional formulation, the vigor of convection is dependent upon the Rayleigh number, *Ra*

$$Ra = \frac{\Delta\rho g H k}{\mu_0\ \kappa} \tag{9}$$

where $\Delta\rho$ is the density contrast between the cold fluids that enter the model and the hot fluids at its base, H is the height of the system, μ_o is the viscosity of basal fluids, and κ is the rock thermal diffusivity which we assumed to be 10^{-6} m^2 s^{-1}. Computational considerations limit our solutions to *Ra*

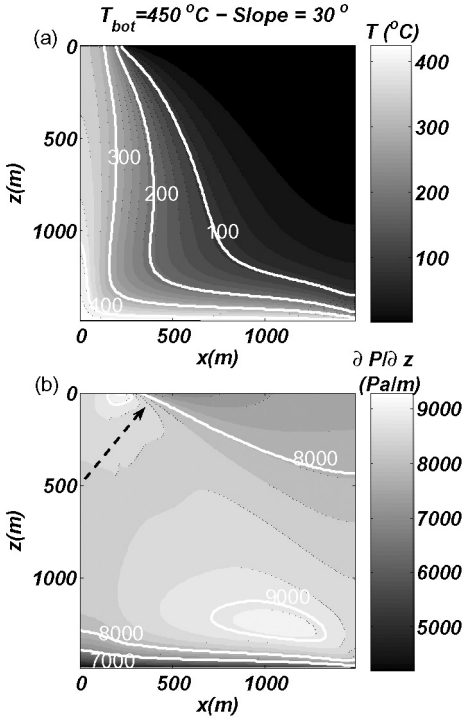

Figure 12. (a) Temperature and (b) vertical pressure gradients in a system with a base that slopes at 30°. The dashed arrow indicates the actual vertical direction. The bottom temperature is set to 450°C. Exit temperatures are about 350°C. Pressure gradients exceed 8000 Pa m^{-1} in most of the upflow zone.

ranging from 200 up to 1000. Because it is difficult to compare Rayleigh numbers for solutions computed at different basal temperatures we also parameterize the vigor of convection with the Nusselt number *Nu* which is defined as the ratio of the observed vertical heat transport to that which would occur by conduction alone.

[38] Figure 10 shows the temperatures and vertical pressure gradients for two models with $Nu \sim 3.5$ and basal temperatures of 400°C and 600°C. The circulation consists of two upwelling zones on the side of the box and one central downwelling zone. The vertical pressure gradients decrease with depth and are the smallest in the bottom boundary layer. When the basal temperature is 400°C, exit temperatures are only 220°C and downwelling fluid temperature ranges from 2°C to 150°C (Figure 10a). Except near the base, pressure gradients are >8000 Pa m^{-1} and are slightly lower in the upwelling zones than in the downwelling one (Figure 10b). When the basal temperature is 600°C the vent temperature is ~380°C and downwelling temperatures are between 2°C and ~250°C (Figure 10c). The vertical pressure gradients are much smaller and do not exceed 7000 Pa m^{-1} in the upflow zone except at the top of the box (Figure 10d).

[39] The solutions above were obtained for fairly low Nusselt numbers. Figure 11 summarizes the results of a series of runs at *Ra* between 200 and 800 for basal temperatures of 400°C and 600°C. Figure 11 shows the local vertical pressure gradients and hydrostatic pressure gradients in the center of the upflow zone as well as the local cold hydrostatic pressure gradients in downflow regions at a depth equal to three quarters of the thickness of the model. The mean pressure gradients are closer to cold hydrostatic than hot hydrostatic pressure gradients. The vertical pressure gradients show consistent trends with increasing Nusselt numbers. Provided the number of circulation cells in the solution remains unchanged the pressure gradients increase with *Nu*. However, when the number of cells increases the pressure gradients drop.

[40] There are several factors that can increase these pressure gradients and hence the salinity of neutrally buoyant brines. Our models are limited to a maximum Rayleigh number of 800 which is equivalent to a permeability $k \leq 6 \times 10^{-15}$ m^2. This is about 2 orders of magnitude lower than the estimated permeability for black smoker fields [*Lowell and Germanovich*, 1994; *Wilcock and McNabb*, 1995; *Wilcock and Fisher*, 2004]. Since the effect of decreasing the cell ratio acts to counteract the progressive increase in pressure gradients with Rayleigh (or Nusselt) number, it is difficult to predict the cell aspect ratio at such high Rayleigh numbers. If the aspect ratio remains fairly large either because upflow zones are controlled by local geology [e.g., *Curewitz and Karson*, 1997] or because of the effects of a sloping bottom boundary [*Rabinowicz et al.*, 1999], then the vertical pressure gradients may be quite high. Models of anhydrite precipitation [*Lowell and Yao*, 2002]

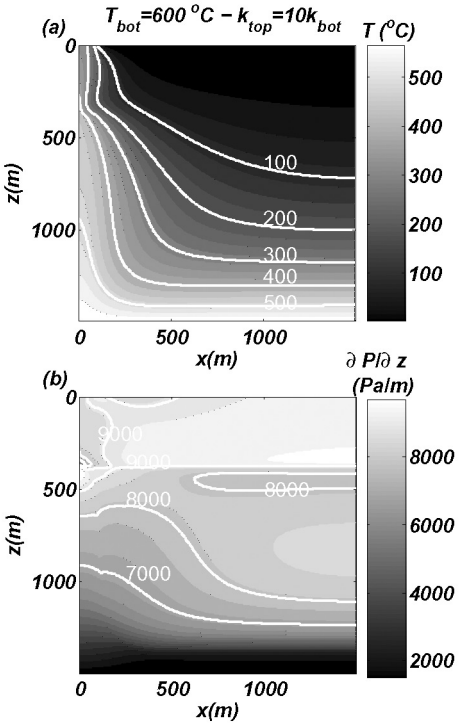

Figure 13. (a) Temperature and (b) vertical pressure gradients in a system in which the upper quarter of the model is 10 times more permeable than the rest. The basal temperature is 600°C, $Nu = 2.5$ and $Ra = 1000$. The upflow zone narrows considerably in the high-permeability zone, and the pressure gradients decrease significantly.

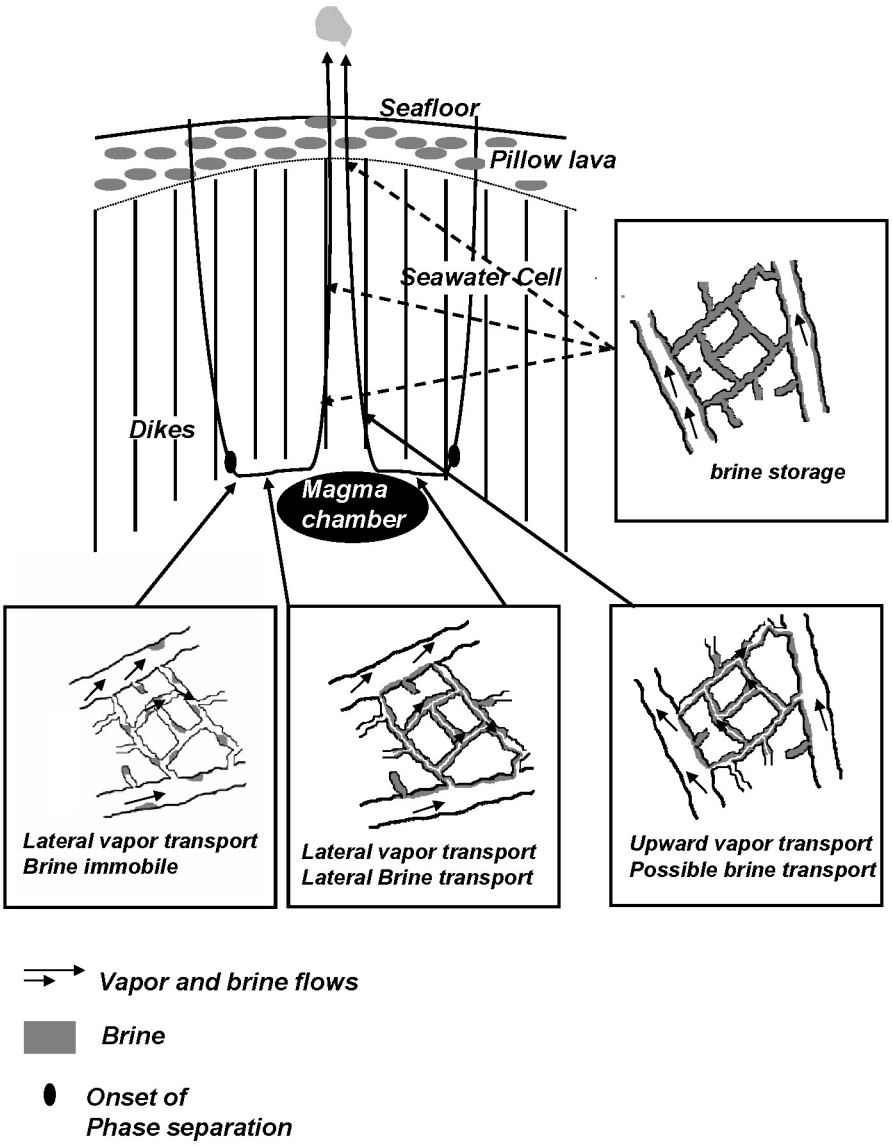

Figure 14. Schematic diagram showing our model for hydrothermal circulation and brine dynamics at mid-ocean ridges.

predict very broad recharge zones and by inference large aspect ratio cells.

[41] Figure 12 illustrates the effect of including a 30° slope at the base of the system. For a given bottom temperature a sloped system will vent higher temperature fluids than a horizontal one [*Rabinowicz et al.*, 1999]. We set the bottom temperature in our slope experiments to 450°C so that venting temperatures are consistent with black smoker systems (350°C). The Rayleigh and Nusselt numbers were 800 and 8, respectively. The convective circulation adopts a single-cell pattern with a broad recharge and a narrow discharge area on the side of the system (Figure 12a). Note that horizontal models with similar Rayleigh and Nusselt numbers are characterized by multiple convective cells (Figure 11). As expected, the large aspect ratio configuration leads to a significant increase in the pressure gradients in the system. In most of the upwelling area fluids with temperature ~400°C are upwelling with pressure gradients >8000 Pa m^{-1}. By comparison, in the experiments with a horizontal base and a bottom temperature of 600°C (Figure 10b), pressure gradients in the upflow zone are ~7000 Pa m^{-1}.

[42] Some caution is required when interpreting pressure gradients derived from single-phase models in terms of the behavior of two-phase systems. However, since the effect of introducing a second phase is to reduce the sum of the two effective permeabilities below the intrinsic permeability (Figure 7), the presence of two phases is likely to lead to an increase in the pressure gradients driving flow in order to balance fluxes with single phase regions.

[43] Our numerical models support the inference of previous studies that mid-ocean ridge hydrothermal systems circulate at pressure gradients that are close to cold hydrostatic. For the models that reproduce black smoker vent

temperature, when the base is flat and at 600°C the pressure gradients of 7000 Pa m^{-1} are equivalent to neutrally buoyant brines with salinities of 10–15 wt % NaCl (Figure 9); when the base is sloped and set to 450°C the pressure gradients of 8000 Pa m^{-1} are equivalent to neutrally buoyant brines with salinities of 15–20 wt % NaCl (Figure 9).

[44] One obvious criticism of models that predict that high-salinity brines are buoyant is the observation that the maximum salinity of vent fluids is limited to 6–7 wt % NaCl [*VonDamm*, 1995]. At seafloor pressures of 250–300 bars, fluids with temperatures of 350°C and with salinities ranging between 10 and 20 wt % NaCl have densities ranging between 770 and 880 kg m^{-3} [*Palliser and McKibbin*, 1998b] and should vent in a system with pressure gradients near cold hydrostatic. However, such interpretation ignores the effect of vertical permeability variations. Figure 13 illustrates the effect of including a high-permeability layer in the upper quarter of the model to simulate the effect of layer 2A. The Rayleigh number computed with the permeability of the bottom layer is 1000 and the permeability increases tenfold in the upper layer. Both the width of the upflow zone and the maximum upwelling temperatures decrease markedly across the permeability boundary. The pressure gradients drop from 8500–9000 Pa m^{-1} immediately below the interface to 5500–6000 Pa m^{-1} above it. We infer that the permeability contrast at the interface between the dike and pillow layers may act as a brine filter with denser fluids accumulating below the interface and lighter ones crossing it.

5. A New Model for Brine Storage

[45] On the basis of the results of this study, we propose a new model for the dynamics and storage of brine in mid-ocean ridge hydrothermal systems (Figure 14). Seawater descends as a single-phase fluid in the recharge area before encountering the bottom thermal boundary layer (reaction zone) where its temperature increases quickly at almost constant pressure until it undergoes supercritical phase separation and forms a brine and a vapor. As a result of interfacial tensions, the newly formed brine segregates from the vapor and preferentially wets the crack walls and fills small fissures, dead ends and backwater porosity while the vapor flows efficiently in the larger fissures. At small volume fractions the brine will remain stagnant as isolated droplets and as its volume increases it will move locally.

[46] Both brine and vapor will then flow horizontally within the bottom thermal boundary layer. If the brines are too dense to rise in the upflow zone then we argue that the high heat fluxes of mid-ocean ridge systems are incompatible with the formation of a separate brine layer. Seawater must continue to circulate to near the base of the permeable crack network and the vapor created by phase separation must move efficiently through brine-rich regions into the upflow zone.

[47] We infer that the pressure gradients within the upflow zone may be sufficiently high that the brines will move up with the vapor. The brines will rise much more slowly than the vapor because of their smaller buoyancy, higher viscosity and the lower effective permeability for the flow in smaller cracks. As brines move up in the discharge area, they eventually reach a level of neutral buoyancy either because they cool or enter a layer of higher permeability where the pressure gradients are reduced. The buoyant vapors rise efficiently through the system via the main fissures and may have little opportunity to mix and equilibrate with the brine before venting at the seafloor. If two-phase flow continues for long periods the whole upflow zone could conceivably become saturated with a brine phase stored up to the base of layer 2A with vapor confined to a few of the widest cracks. When the vapor production stops because the system cools to the one-phase region, the brines could settle to form a layered system. These brines slowly mix with hydrothermal fluids of seawater salinity flowing in the widest fissures to produce the high-salinity fluids observed at some hydrothermal vents.

[48] **Acknowledgments.** We thank Robert Detrick and Wenyue Xu for their thorough reviews of earlier versions of this manuscript and Deborah Kelley, Marvin Lilley, David Butterfield, Russell McDuff, and Michel Rabinowicz for helpful discussions. Publication of this work was supported by grant OCE-0243395 from the National Science Foundation.

References

Anderko, A., and K. S. Pitzer (1993), Equation-of-state representation of phase equilibria and volumetric properties of the system NaCl-H_2O above 573°K, *Geochim. Cosmochim. Acta*, *57*, 1657–1680.

Bai, W., W. Xu, and R. P. Lowell (2003), The dynamics of submarine geothermal heat pipes, *Geophys. Res. Lett.*, *30*(3), 1108, doi:10.1029/2002GL016176.

Becker, K. (1985), Large-scale electrical resistivity and bulk porosity of the oceanic crust, Deep Sea Drilling Project hole 504B, *Initial Rep. Deep Sea Drill. Proj.*, *83*, 419–427.

Bischoff, J. L., and R. J. Rosenbauer (1989), Salinity variations in submarine hydrothermal systems by layered double-diffusive convection, *J. Geol.*, *97*, 613–623.

Bosch, D., M. Jamais, F. Boudier, A. Nicolas, J.-M. Dautria, and P. Agrinier (2004), Deep and high-temperature hydrothermal circulation in the Oman ophiolite- petrological and isotopic evodence, *J. Petrol.*, *45*, 1181–1208.

Brooks, R. H., and A. T. Corey (1964), Hydraulic properties of porous media, *Hydrol. Pap.*, *3*, 1–27.

Burdine, N. T. (1953), Relative permeability calculation from size distribution data, *Trans. Am. Inst. Mech. Eng.*, *198*, 71–78.

Butterfield, D. A., and G. J. Massoth (1994), Geochemistry of North Cleft segment vent fluids: Temporal changes in chlorinity and their possible relation to recent volcanism, *J. Geophys. Res.*, *99*, 4951–4968.

Butterfield, D. A., G. J. Massoth, R. E. McDuff, J. E. Lupton, and M. D. Lilley (1990), The geochemistry of hydrothermal fluids from ASHES vent field, Axial Seamount, Juan de Fuca Ridge: Subseafloor boiling and subsequent fluid-rock interaction, *J. Geophys. Res.*, *95*, 12,895–12,922.

Butterfield, D. A., R. E. McDuff, M. J. Mottl, M. D. Lilley, J. E. Lupton, and G. J. Massoth (1994), Gradients in the composition of hydrothermal fluids from the Endeavour segment vent field: Phase separation and brine loss, *J. Geophys. Res.*, *99*, 9561–9583.

Butterfield, D. A., I. R. Jonasson, G. J. Massoth, R. A. Feely, K. K. Roe, R. E. Embley, J. F. Holden, R. E. McDuff, M. D. Lilley, and J. R. Delaney (1997), Seafloor eruptions and evolution of hydrothermal fluid chemistry, *Philos. Trans. R. Soc. London, Ser. A*, *355*, 369–386.

Cann, J., and M. R. Strens (1989), Modeling periodic megaplume emission by black smoker systems, *J. Geophys. Res.*, *94*, 12,227–12,237.

Chen, Y. J. (2004), Modeling the thermal state of the oceanic crust, in *Mid-Ocean Ridges: Hydrothermal Interactions Between the Lithosphere and Oceans*, *Geophys. Monogr. Ser.*, vol. 148, edited by C. R. German et al., pp. 65–78, AGU, Washington, D. C.

Cherkaoui, A. S. M., W. S. D. Wilcock, R. A. Dunn, and D. R. Toomey (2003), A numerical model of hydrothermal cooling and crustal accretion at a fast spreading mid-ocean ridge, *Geochem. Geophys. Geosyst.*, *4*(9), 8616, doi:10.1029/2001GC000215.

Cowan, J., and J. Cann (1988), Supercritical two-phase separation of hydrothermal fluids in the Troodos ophiolite, *Nature*, *333*, 259–261.

Crawford, W. C., and S. C. Webb (2002), Variations in the distribution of magma in the lower crust and at the Moho beneath the East Pacific Rise at 9°–10°N, *Earth Planet. Sci. Lett.*, *203*, 117–130.

Curewitz, D., and J. A. Karson (1997), Structural settings of hydrothermal flow: Permeability maintained by fault propagation and interaction, *J. Volcanol. Geotherm. Res.*, *79*, 149–168.

Delaney, J. R., D. W. Mogk, and M. J. Mottl (1987), Quartz-cemented breccias from the Mid-Atlantic Ridge: Samples of a high-salinity hydrothermal upflow zone, *J. Geophys. Res.*, *92*, 9175–9192.

Delaney, J. R., V. Robigou, R. E. McDuff, and M. K. Tivey (1992), Geology of a vigorous hydrothermal system on the Endeavour segment, Juan de Fuca Ridge, *J. Geophys. Res.*, *97*, 19,663–19,682.

Detrick, R. S., P. Buhl, E. Vera, J. Mutter, J. Orcutt, J. Madsen, and T. Brocher (1987), Multichannel seismic imaging of a crustal magma chamber along the East Pacific Rise between 9°N and 13°N, *Nature*, *326*, 35–41.

Detrick, R. S., S. Carbotte, E. Van Ark, J. P. Canales, G. Kent, A. Harding, J. Diebold, and M. Nedimovic (2002), New multichannel seismic constraints on the crustal structure of the Endeavour Segment, Juan de Fuca Ridge: Evidence for a crustal magma chamber, *Eos Trans. AGU*, *83*(47), Fall Meet. Suppl., Abstract T12B-1316.

Driesner, T., and C. A. Heinrich (2003), Accurate P-T-X-V-H correlations for the system NaCl-H_2O from 0 to 800°C, 0 to 500 MPa, and 0 to 1 XNaCl, *Acta Mineral. Pet. Abstr. Ser.*, *2*, 55–56.

Driesner, T., T. M. Seward, and G. Tironi (1991), Molecular dynamics simulation of ionic hydration and ion association in dilute and 1 molal aqueous sodium chloride solutions from ambient to supercritical conditions, *Geochim. Cosmochim. Acta*, *62*, 3095–3107.

Dunn, R. A., D. R. Toomey, and S. C. Solomon (2000), Three-dimensional seismic structure and physical properties of the crust and shallow mantle beneath the East Pacific Rise at 9°30′N, *J. Geophys. Res.*, *105*, 23,537–23,556.

Edmond, J. M., C. Measure, R. E. McDuff, L. H. Chan, R. Collier, B. Grant, L. I. Gordon, and J. B. Corliss (1979), Ridge crest hydrothermal activity and the balances of the major and minor elements in the ocean: The Galapagos data, *Earth Planet. Sci. Lett.*, *46*, 1–18.

Faust, C. R., and J. W. Mercer (1979), Geothermal reservoir simulation: 1. Mathematical models for liquid- and vapor-dominated hydrothermal systems, *Water Resour. Res.*, *15*, 23–30.

Fontaine, F. J., M. Rabinowicz, and J. Boulègue (2001), Permeability changes due to mineral diagenesis in fractured crust: Implications for hydrothermal circulation at mid-ocean ridges, *Earth Planet Sci. Lett.*, *184*, 407–425.

Fox, C. G. (1990), Consequences of phase separation on the distribution of hydrothermal fluids at ASHES vent field, Axial Volcano, Juan de Fuca Ridge, *J. Geophys. Res.*, *95*, 12,923–12,926.

Geiger, S., T. Driesner, C. A. Heinrich, and S. K. Matthai (2004), On the effects of NaCl on convective fluid-flow in magmatic-hydrothermal systems, *Eos Trans. AGU*, *85*(47), Fall Meet. Suppl., Abstract V31A-1414.

German, C. R., and J. Lin (2004), The thermal structure of the oceanic crust, ridge-spreading and hydrothermal circulation: How well do we understand their inter-connections?, in *Mid-Ocean Ridges: Hydrothermal Interactions between the Lithosphere and Oceans*, *Geophys. Monogr. Ser.*, vol. 148, edited by C. R. German et al., pp. 1–18, AGU, Washington, D. C.

Gillis, K. M., K. Muehlenbachs, M. Stewart, T. Gleeson, and J. Karson (2001), Fluid flow patterns in fast spreading East Pacific Rise crust exposed at Hess Deep, *J. Geophys. Res.*, *106*, 26,311–26,330.

Goldfarb, M. S., and J. R. Delaney (1988), Response of two-phase fluids to fracture configurations within submarine hydrothermal systems, *J. Geophys. Res.*, *93*, 4585–4594.

Griffiths, R. W. (1981), Layered double-diffusive convection in porous media, *J. Fluid Mech.*, *102*, 221–248.

Hayba, D. O., and S. E. Ingebritsen (1997), Multiphase groundwater flow near a cooling plutons, *J. Geophys. Res.*, *102*, 12,235–12,252.

Helmig, R. (1997), *Multiphase Flow and Transport Processes in the Subsurface*, Springer, New York.

Hirth, G., J. Escartin, and J. Lin (1998), The rheology of the lower oceanic crust: Implications for lithospheric deformation at mid-ocean ridges, in *Faulting and Magmatism at Mid-Ocean Ridges*, *Geophys. Monogr. Ser.*, vol. 106, edited by W. R. Buck et al., pp. 291–303, AGU, Washington, D. C.

Horne, R. N., C. Satik, G. Mahiya, K. Li, W. Ambusso, R. Tovar, C. Wang, and H. Nassori (2000), Steam-water relative permeability, paper presented at World Geothermal Congress, Int. Geotherm. Assoc., Kyushu, Japan.

Ingebritsen, S. E., and D. O. Hayba (1994), Fluid flow and heat transport near the critical point of H_2O, *Geophys. Res. Lett.*, *21*, 2199–2202.

Johnson, H. P., M. Hutnak, R. P. Dziak, C. G. Fox, I. Uroyo, J. P. Cowen, J. Nabelek, and C. Fisher (2000), Earthquake-induced changes in a hydrothermal system at the Endeavour segment, *Nature*, *407*, 174–177.

Jupp, T., and A. Schultz (2004), Physical balances in subseafloor hydrothermal convection cells, *J. Geophys. Res.*, *109*, B05101, doi:10.1029/2003JB002697.

Kawada, Y., S. Yoshida, and S. Watanabe (2004), Numerical simulations of mid-ocean ridge hydrothermal circulation including the phase separation of seawater, *Earth Planets Space*, *56*, 193–215.

Kelley, D. S., and G. L. Früh-Green (2001), Volatile lines of descent in submarine plutonic environments: Insights from stable isotope and fluid inclusion analyses, *Geochim. Cosmochim. Acta*, *65*, 3325–3346.

Kelley, D. S., P. T. Robinson, and J. G. Malpas (1992), Processes of brine generation and circulation in the oceanic crust: Fluid inclusion evidence from the Troodos Ophiolite, Cyprus, *J. Geophys. Res.*, *97*, 9307–9322.

Kelley, D. S., K. M. Gillis, and G. Thompson (1993), Fluid evolution in submarine magma-hydrothermal systems at the Mid-Atlantic Ridge, *J. Geophys. Res.*, *98*, 19,579–19,596.

Kent, G. M., A. J. Harding, and J. A. Orcutt (1990), Evidence for a smaller magma chamber beneath the East Pacific Rise at 9°30′N, *Nature*, *344*, 650–653.

Lewis, K. C., and R. P. Lowell (2004), Mathematical modeling of phase separation of seawater near an igneous dike, *Geofluids*, *4*, 197–209.

Lilley, M. D., D. A. Butterfield, J. E. Lupton, and E. J. Olson (2003), Magmatic events can produce repid changes in hydrothermal vent chemistry, *Nature*, *422*, 878–881.

Lowell, R. P., and L. N. Germanovich (1994), On the temporal evolution of high-temperature hydrothermal systems at ocean ridge crest, *J. Geophys. Res.*, *99*, 565–576.

Lowell, R. P., and L. N. Germanovich (1997), Evolution of a brine-saturated layer at the base of a ridge-crest hydrothermal system, *J. Geophys. Res.*, *102*, 10,245–10,256.

Lowell, R. P., and L. N. Germanovich (2004), Hydrothermal processes at mid-ocean ridges: Results from scale analysis and single-pass models, in *Mid-Ocean Ridges: Hydrothermal Interactions Between the Lithosphere and Oceans*, *Geophys. Monogr. Ser.*, vol. 148, edited by C. R. German et al., pp. 110–127, AGU, Washington, D. C.

Lowell, R. P., and Y. Yao (2002), Anhydrite precipitation and the extent of hydrothermal recharge zones at ocean ridge crests, *J. Geophys. Res.*, *107*(B9), 2183, doi:10.1029/2001JB001289.

Magde, L. S., A. H. Barclay, D. R. Toomey, R. S. Detrick, and J. A. Collins (2000), Crustal magma plumbing within a segment of the Mid-Atlantic Ridge, 35°N, *Earth and Planet. Sci. Lett.*, *175*, 55–67.

Magenheim, A. J., A. J. Spivak, P. J. Michael, and J. M. Gieskes (1995), Chlorine stable isotope composition of the oceanic crust: Implications for Earth's distribution of chlorine, *Earth. Planet. Sci. Lett.*, *131*, 427–432.

Manning, C. E., P. E. Weston, and K. I. Mahon (1996), Rapid high-temperature metamorphism of East Pacific Rise gabbros from Hess Deep, *Earth and Planet. Sci. Lett.*, *144*, 123–132.

Manning, C. E., C. MacLeod, and P. E. Weston (2000), Lower-crustal cracking front at fast-spreading ridges: Evidence from the East Pacific Rise and the Oman ophiolite, *Spec. Pap. Geol. Soc. Am.*, *349*, 261–272.

McNabb, A., and J. Fenner (1985), Thermohaline convection beneath the ocean floor, paper presented at CSIRO/DSIR Seminar on convective flows in porous media, Dep. of Sci. and Ind. Res., Wellington, New Zealand.

Meyer, C. A., R. B. McClintock, G. J. Silvestri, and R. C. Spencer Jr. (1993), *ASME Steam Table: Thermodynamic and Transport Properties of Steam*, Am. Soc. of Mech. Eng., New York.

Michael, P. J., and W. C. Cornell (1998), Influence of spreading rate and magma supply on crystallization and assimilation beneath mid-ocean ridges: Evidence from chlorine and major element chemistry of mid-ocean ridge basalts, *J. Geophys. Res.*, *103*, 18,325–18,356.

Mualem, Y. (1976), A new model for predicting the hydraulic conductivity of unsaturated porous media, *Water Resour. Res.*, *12*, 593–622.

Nehlig, P. (1991), Salinity of oceanic hydrothermal fluids: A fluid inclusion study, *Earth Planet. Sci. Lett.*, *102*, 310–325.

Nicolas, A., D. Mainprice, and F. Boudier (2003), High-temperature seawater circulation throughout crust of oceanic ridges: A model derived from the Oman ophiolites, *J. Geophys. Res.*, *108*(B8), 2371, doi:10.1029/2002JB002094.

Nield, D. A., and N. A. Bejan (1992), *Convection in Porous Media*, Springer, New York.

Oelkers, E. H., and H. C. Helgeson (1991), Calculation of activity coefficients and degrees of formation of neutral ion pairs in supercritical electrolyte solutions, *Geochim. Cosmochim. Acta*, *55*, 1235–1251.

Oelkers, E. H., and H. C. Helgeson (1993), Calculation of dissociation constants and the relative stabilities of polynuclear clusters of 1:1 electrolytes in hydrothermal solutions at supercritical pressures and temperatures, *Geochim. Cosmochim. Acta*, *57*, 2673–2697.

Palliser, C., and R. McKibbin (1998a), A model for deep geothermal brines, I: T-p-X state-space description, *Transp. Porous Media*, *33*, 65–80.

Palliser, C., and R. McKibbin (1998b), A model for deep geothermal brines, II: Thermodynamic properties—Density, *Transp. Porous Media*, *33*, 129–154.

Palliser, C., and R. McKibbin (1998c), A model for deep geothermal brines, III: Thermodynamic properties—Enthalpy and viscosity, *Transp. Porous Media*, *33*, 155–171.

Pitzer, K. S., J. C. Peiper, and R. H. Busey (1984), Thermodynamic properties of aqueous sodium chloride solutions, *J. Phys. Chem. Ref. Data*, *13*, 1–106.

Rabinowicz, M., J. Boulègue, and P. Genthon (1998), Two and three-dimensional modeling of hydrothermal convection in the sedimented Middle Valley segment, Juan de Fuca Ridge, *J. Geophys. Res.*, *103*, 24,045–24,065.

Rabinowicz, M., J.-C. Sempéré, and P. Genthon (1999), Thermal convection in a vertical permeable slot: Implications for hydrothermal circulation along mid-ocean ridges, *J. Geophys. Res.*, *104*, 29,275–29,292.

Romm, E. S. (1966), *Fluid Flow in Fractured Rocks*, Nedra, Moscow.

Saccocia, P. J., and K. M. Gillis (1995), Hydrothermal upflow zones in the oceanic crust, *Earth Planet. Sci. Lett.*, *136*, 1–16.

Scholl, M. A., S. E. Ingebritsen, and H. I. Essaid (1993), Comment on "Consequences of phase separation on the distribution of hydrothermal fluids at ASHES vent field, axial volcano, Juan de Fuca Ridge" by Christopher G. Fox, *J. Geophys. Res.*, *98*, 1813–1815.

Schoofs, S., and U. Hansen (2000), Depletion of a brine layer at the base of ridge-crest hydrothermal systems, *Earth Planet Sci. Lett.*, *180*, 341–353.

Schoofs, S., R. A. Trompert, and U. Hansen (1998), The formation and evolution of layered structures in porous media, *J. Geophys. Res.*, *103*, 20,843–20,858.

Schoofs, S., R. A. Trompert, and U. Hansen (2000), The formation and evolution of layered structures in porous media: Effects of porosity and mechanical dispersion, *Phys. Earth Planet. Inter.*, *118*, 205–225.

Seyfried, W. E., Jr., M. E. Berndt, and D. R. Janecky (1986), Chloride depletion and enrichments in seafloor hydrothermal fluids: Constraints from experimental basalt alteration studies, *Geochim. Cosmochim. Acta*, *50*, 469–475.

Seyfried, W. E., Jr., J. S. Seewald, M. E. Berndt, K. Ding, and D. I. Foustoukos (2003), Chemistry of hydrothermal vent fluids from the Main Endeavour Field, northern Juan de Fuca Ridge: Geochemical controls in the aftermath of June 1999 seismic events, *J. Geophys. Res.*, *108*(B9), 2429, doi:10.1029/2002JB001957.

Singh, S. C., G. M. Kent, J. S. Collier, A. J. Harding, and J. A. Orcutt (1998), Melt to mush variations in crustal magma properties along the ridge crest at the southern East Pacific Rise, *Nature*, *394*, 874–878.

Singh, S. C., J. S. Collier, A. J. Harding, G. M. Kent, and J. A. Orcutt (1999), Seismic evidence for a hydrothermal layer above the solid roof of the axial magma chamber at the southern East Pacific Rise, *Geology*, *27*, 219–222.

Sinha, M. C., D. A. Navin, L. M. McGregor, S. Constable, C. Peirce, A. White, G. Heinson, and M. A. Inglis (1997), Evidence for accumulated melt beneath the slow-spreading Mid-Atlantic Ridge, *Philos. Trans. R. Soc., Ser. A*, *355*, 233–253.

Stumm, W. (1992), *Chemistry of the Solid-Water Interface: Processes at the Mineral-Water and Particle-Water Interface in Natural Systems*, John Wiley, Hoboken, N. J.

Toomey, D. R., S. C. Solomon, G. M. Purdy, and M. H. Murray (1985), Microearthquakes beneath the median valley of the Mid-Atlantic Ridge near 23°N: Hypocenters and focal mechanisms, *J. Geophys. Res.*, *90*, 5443–5458.

Toomey, D. R., S. C. Solomon, and G. M. Purdy (1994), Tomographic imaging of the shallow crustal structure of the East Pacific Rise at 9°30′N, *J. Geophys. Res.*, *99*, 24,135–24,157.

Van Ark, E. M., R. S. Detrick, J. P. Canales, S. Carbotte, J. Diebold, A. Harding, G. Kent, M. Nedimovic, and W. S. Wilcock (2003), Seismic structure of the Endeavour Segment, Juan de Fuca Ridge: Correlations of crustal magma chamber properties with seismicity, faulting, and hydrothermal activity, *Eos Trans. AGU*, *84*(46), Fall Meet. Suppl., Abstract B12A-0752.

Van Genutchen, M. T. (1980), A closed-form equation for predicting the hydraulic conductivity of unsaturated soils, *Soil Sci. Soc. Am. J.*, *44*, 892–898.

Vanko, D. A., and D. S. Stakes (1991), Fluids in oceanic layer 3: Evidence from veined rocks, Hole 735B, Southwest Indian Ridge, *Proc. Ocean Drill. Program Sci. Results.*, *118*, 181–215.

Veirs, S. R., F. R. Stahr, R. E. McDuff, R. E. Thomson, D. R. Yoerger, and A. M. Bradley (2001), Measurements and models of heat flux magnitude and variance from the Main Endeavour hydrothermal vent field, *Eos Trans. AGU*, *82*(47), Fall Meet. Suppl., Abstract OS21B-0444.

VonDamm, K. L. (1988), Systematics and postulated controls on submarine hydrothermal solution chemistry, *J. Geophys. Res.*, *93*, 4551–4561.

VonDamm, K. L. (1995), Control on the chemistry and temporal variability of seafloor hydrothermal fluids, in *Seafloor Hydrothermal Systems: Physical, Chemical, Biological and Geological Interactions*, *Geophys. Monogr. Ser.*, vol. 91, edited by S. E. Humphris et al., pp. 222–247, AGU, Washington, D. C.

VonDamm, K. L. (2004), Evolution of the hydrothermal system at East Pacific Rise 9°50′N: Geochemical evidence for changes in the upper oceanic crust, in *Mid-Ocean Ridges: Hydrothermal Interactions Between the Lithosphere and Oceans*, *Geophys. Monogr. Ser.*, vol. 148, edited by C. R. German et al., pp. 285–304, AGU, Washington, D. C.

VonDamm, K. L., and J. L. Bischoff (1987), Chemistry of hydrothermal solutions from the southern Juan de Fuca Ridge, *J. Geophys. Res.*, *92*, 11,334–11,346.

VonDamm, K. L., L. G. Buttermore, S. E. Oosting, A. M. Bray, D. J. Fornari, M. D. Lilley, and W. C. Shanks III (1997), Direct observation of the evolution of a seafloor 'black smoker' from vapor to brine, *Earth Planet Sci. Lett.*, *149*, 101–111.

Wang, C. T., and R. N. Horne (2000), Boiling flow in a horizontal fracture, *Geothermics*, *29*, 759–772.

Wilcock, W. S. D. (1997), A model for the formation of transient event plumes above mid-ocean ridge hydrothermal systems, *J. Geophys. Res.*, *102*, 12,109–12,122.

Wilcock, W. S. D. (1998), Cellular convection models of mid-ocean ridge hydrothermal circulation and the temperatures of black smoker fluids, *J. Geophys. Res.*, *103*, 2585–2596.

Wilcock, W. S. D., and A. T. Fisher (2004), Geophysical constraints on the subseafloor environment near mid-ocean ridges, in *The Subseafloor Biosphere at Mid-Ocean Ridges*, *Geophys. Monogr. Ser.*, vol. 144, edited by W. S. D. Wilcock et al., pp. 51–74, AGU, Washington, D. C.

Wilcock, W. S. D., and A. McNabb (1995), Estimates of crustal permeability on the Endeavour segment of the Juan de Fuca mid-ocean ridge, *Earth Planet. Sci. Lett.*, *138*, 83–91.

Wolfe, C. J., G. M. Purdy, D. R. Toomey, and S. C. Solomon (1995), Microearthquake characteristics and crustal velocity structure at 29°N on the Mid-Atlantic Ridge: The architecture of a slow spreading segment, *J. Geophys. Res.*, *100*, 24,449–24,472.

Xu, W., and R. P. Lowell (1998), Oscillatory instability of one-dimensional two-phase hydrothermal flow in heterogeneous porous media, *J. Geophys. Res.*, *103*, 20,859–20,868.

F. J. Fontaine and W. S. D. Wilcock, School of Oceanography, University of Washington, Box 357940, Seattle, WA 98195-7940, USA. (fontaine@ocean.washington.edu)